Supporting information for

Influence of Aliovalent Substitution on Structure and Dynamics in Sodium Halide $Na_{3-2x}Y_{1-x}Nb_xCl_6$ Solid Electrolytes

Brian B. Phan [a], Tso Shuen [b], Dmitry Vrublevskiy [a], Qingyu Yan [b] and Vladimir K. Michaelis [a,*]

[a] Department of Chemistry, University of Alberta, Edmonton, Alberta, Canada, T6G 2G2

[b] School of Materials Science and Engineering, Nanyang Technological University, Singapore 639798

Table of Contents

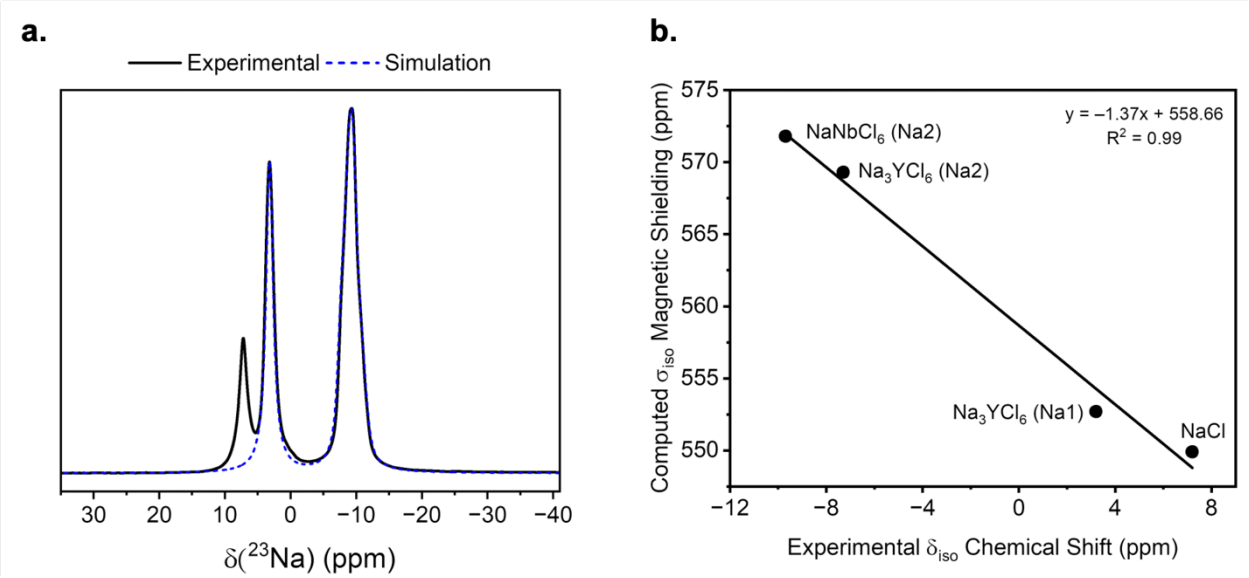

Figure S1. (a) ^{23}Na MAS NMR (B_0 = 11.7 T, ν_{rot} = 10 kHz) of Na_3YCl_6 simulations (dashed blue line) of octahedral and prismatic sites overlayed on top of experimental (black) data. (b) Plot of ^{23}Na magnetic shielding values computed from CASTEP against experimental isotropic chemical shifts of NaCl, Na_3YCl_6, and $NaNbCl_6$.

Table S1. Experimental and GIPAW DFT computed ^{23}Na NMR shielding parameters for Na_3YCl_6 and $NaNbCl_6$.

Sample	δ_{iso} (ppm)		C_Q (MHz)		η	
	Experimental	Computed[a]	Experimental	Computed	Experimental	Computed
Na_3YCl_6	3.2(3)	5.9	0.0(2)	0.9	0.1(6)	0.45
	–7.3(3)	–10.6	1.0(3)	1.3	0.6(9)	0.65
$NaNbCl_6$	–9.7(3)	–13.1	0.0(3)	0.9	0.0(1)	0.6

[a] ^{23}Na magnetic shielding tensors were converted into chemical shift values using $\delta(ppm) \approx \sigma_{ref}(ppm) - \sigma_{DFT}(ppm)$, where σ_{ref} = 558.6 ppm was used based on the relationship of NaCl and the end member.

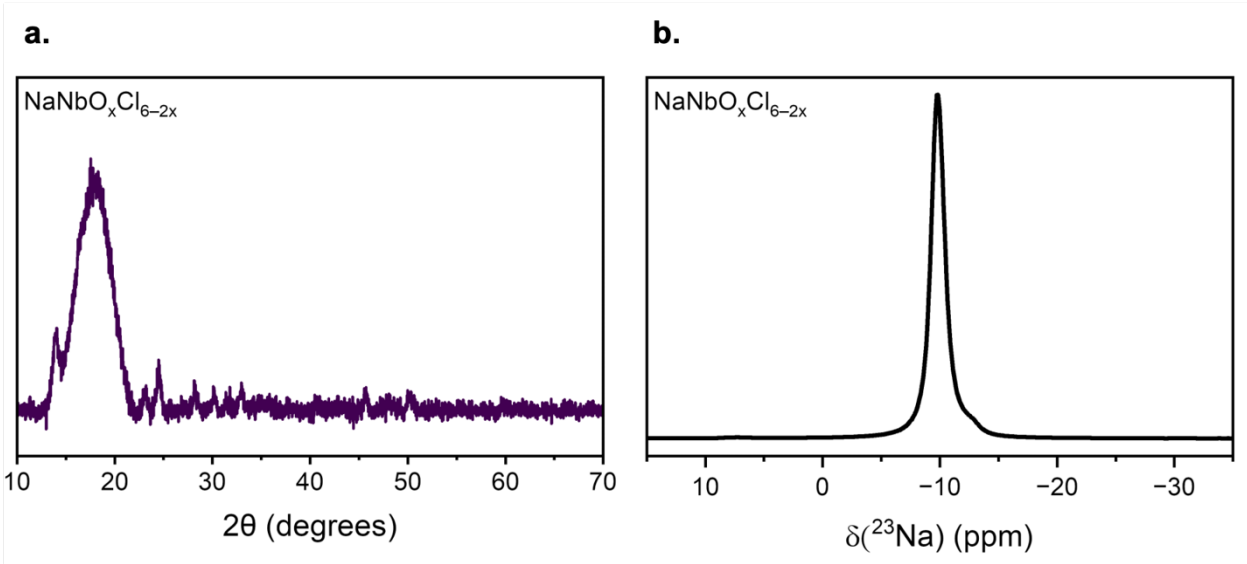

Figure S2. (a) PXRD and (b) ^{23}Na MAS NMR (B_0 = 18.8 T, ν_{rot} = 10 kHz) of $NaNbO_xCl_{6-2x}$.

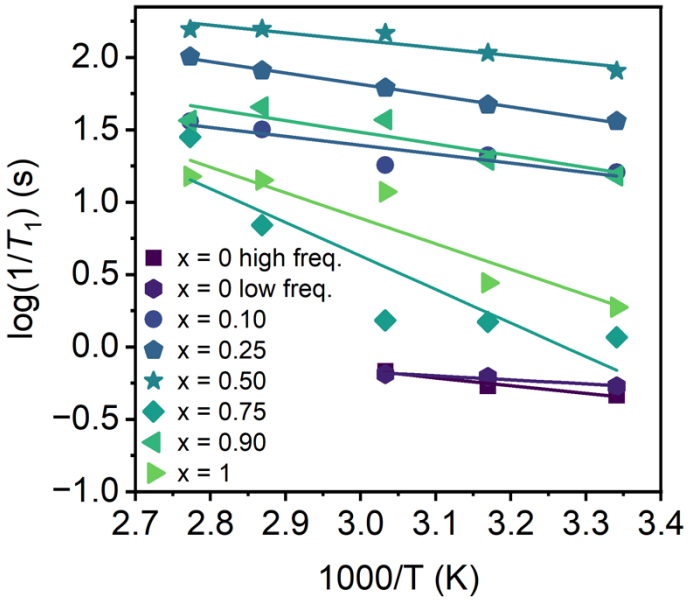

Figure S3. Arrhenius plot of local Na-ion hopping rates derived from spin-lattice relaxation rates as a function of 1000/T.

Table S2. Activation energies extracted from ^{23}Na VT NMR of $Na_{3-2x}Y_{1-x}Nb_xCl_6$ series.

Sample	E_a VT NMR (eV)
Na_3YCl_6	0.04(6) @ 3.2 ppm 0.02(4) @ –9.1 ppm
$Na_{2.8}Y_{0.90}Nb_{0.10}Cl_6$	0.05(3)
$Na_{2.5}Y_{0.75}Nb_{0.25}Cl_6$	0.06(6)
$Na_2Y_{0.50}Nb_{0.50}Cl_6$	0.04(5)
$Na_{1.5}Y_{0.25}Nb_{0.75}Cl_6$	0.19(9)
$Na_{1.2}Y_{0.10}Nb_{0.90}Cl_6$	0.06(9)
$NaNbCl_6$	0.15(1)

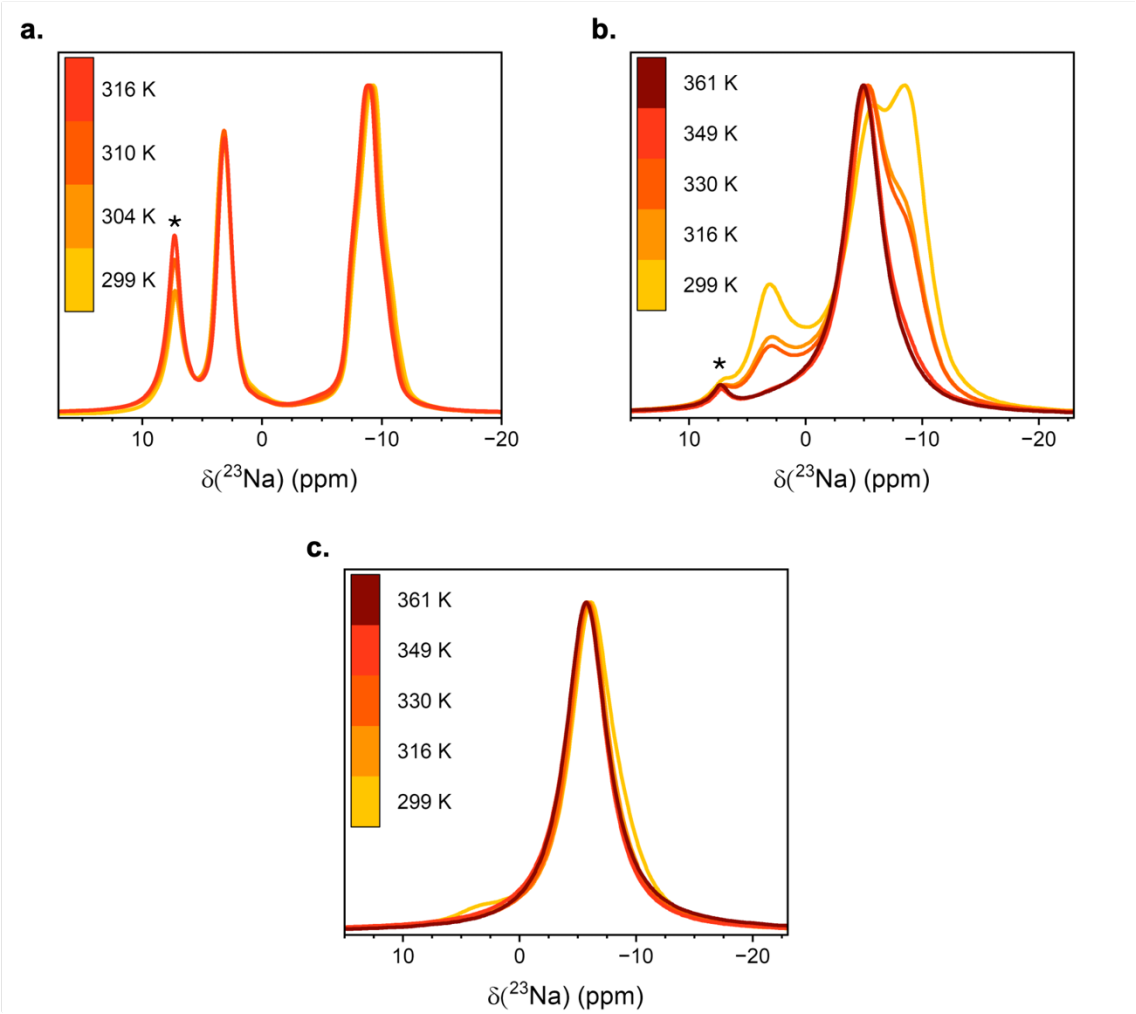

Figure S4. VT ^{23}Na MAS NMR spectra (B_0 = 11.7 T, ν_{rot} = 10 kHz) of (a) YNb0 (b) YNb10 and (c) YNb25. Asterisk (*) indicates NaCl impurity.

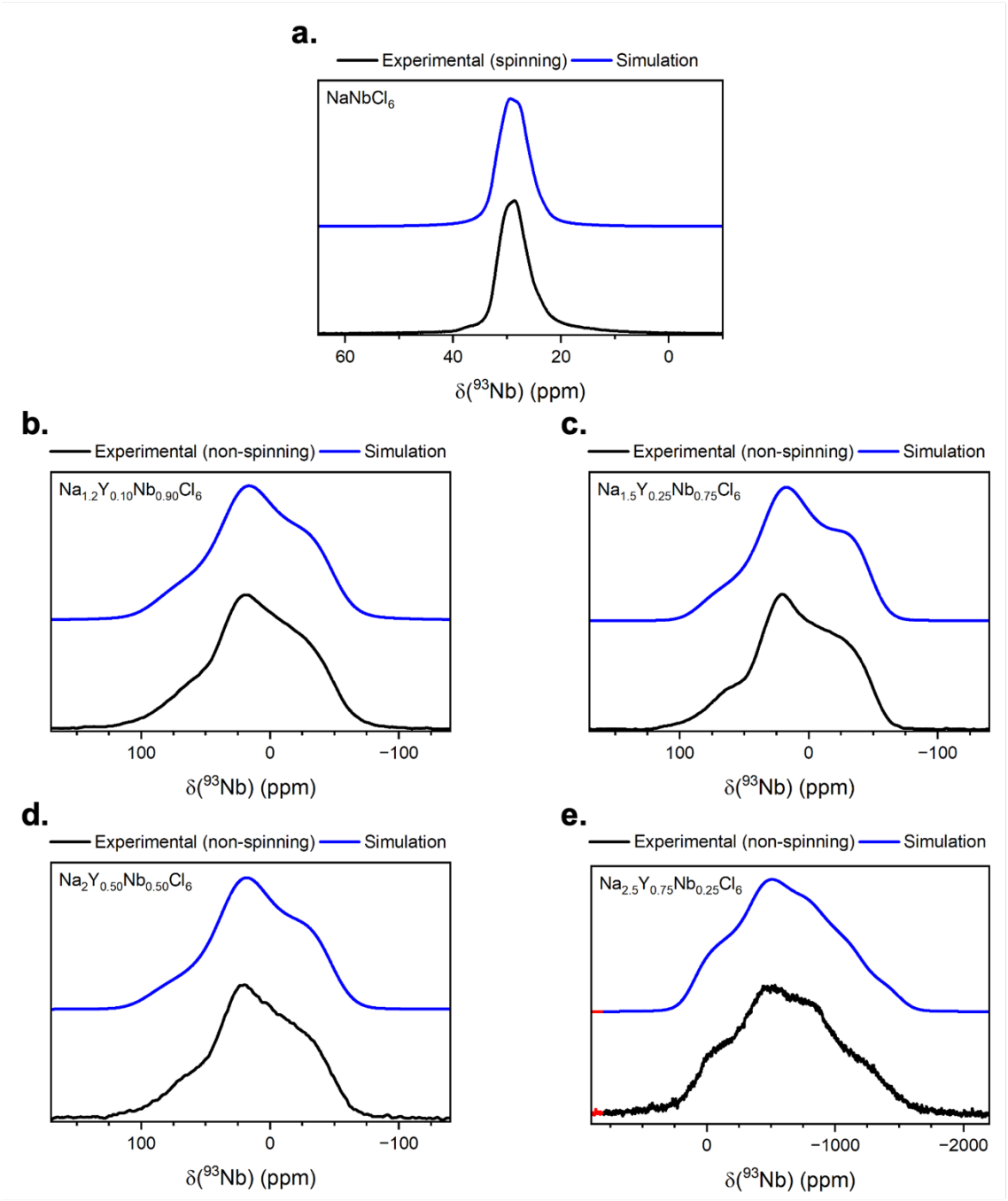

Figure S5. ^{93}Nb NMR spectra of (a) $NaNbCl_6$ acquired at $B_0 = 18.8$ T ($\nu_{rot} = 22$ kHz). Non-spinning ^{93}Nb NMR spectra ($B_0 = 11.7$ T) of (b) YNb90, (c) YNb75, (d) YNb50, and (e) YNb25 ($B_0 = 18.8$ T).

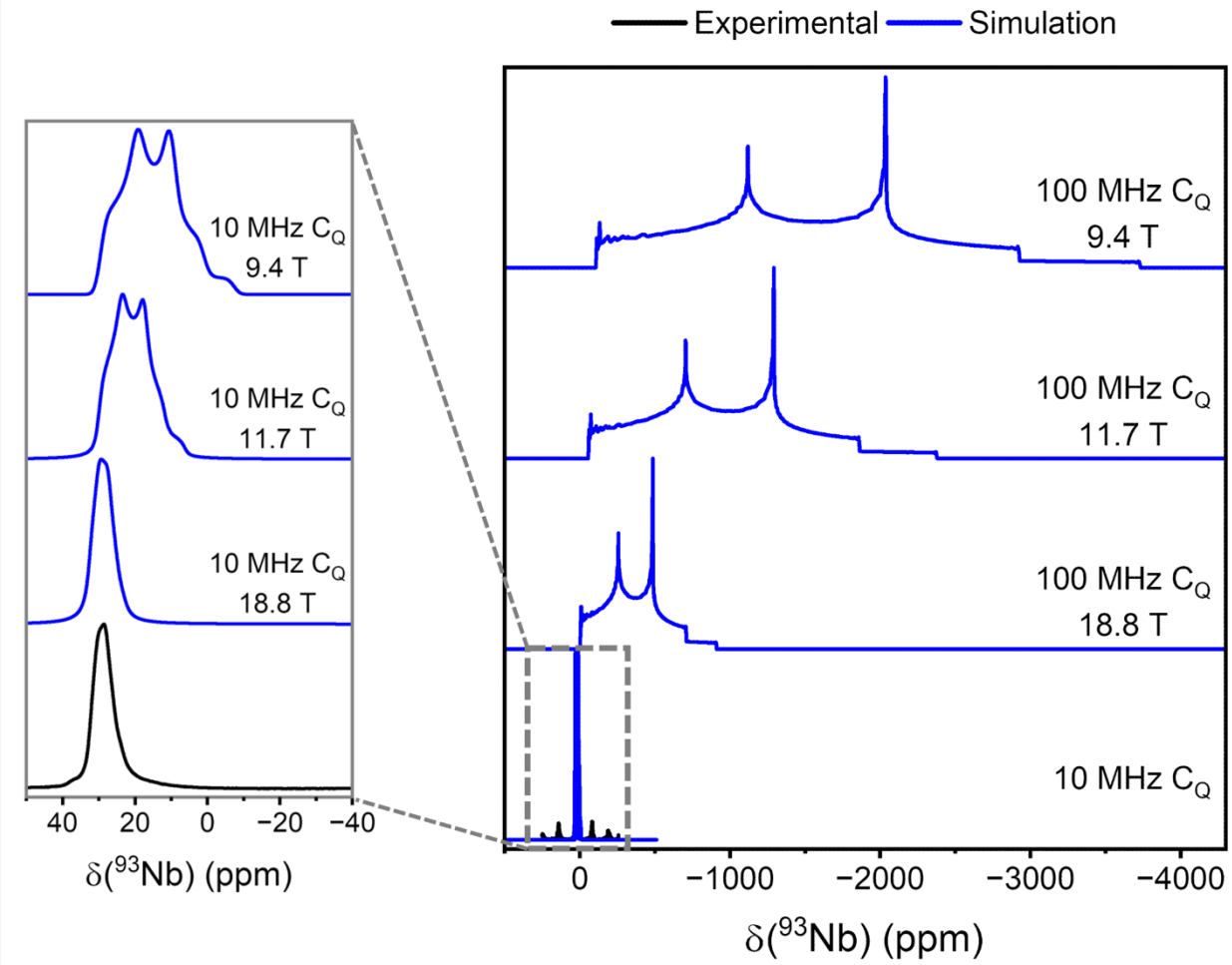

Figure S6. ^{93}Nb MAS NMR of $NaNbCl_6$ (experimental, ν_{rot} = 22 kHz; simulation, $\nu_{rot} = \infty$) simulated at 9.4 T, 11.7 T, and 18.8 T with either C_Q = 10 or 100 MHz. For consistency, η = 0.47 and δ_{iso} = 30 ppm were used across the various simulations.

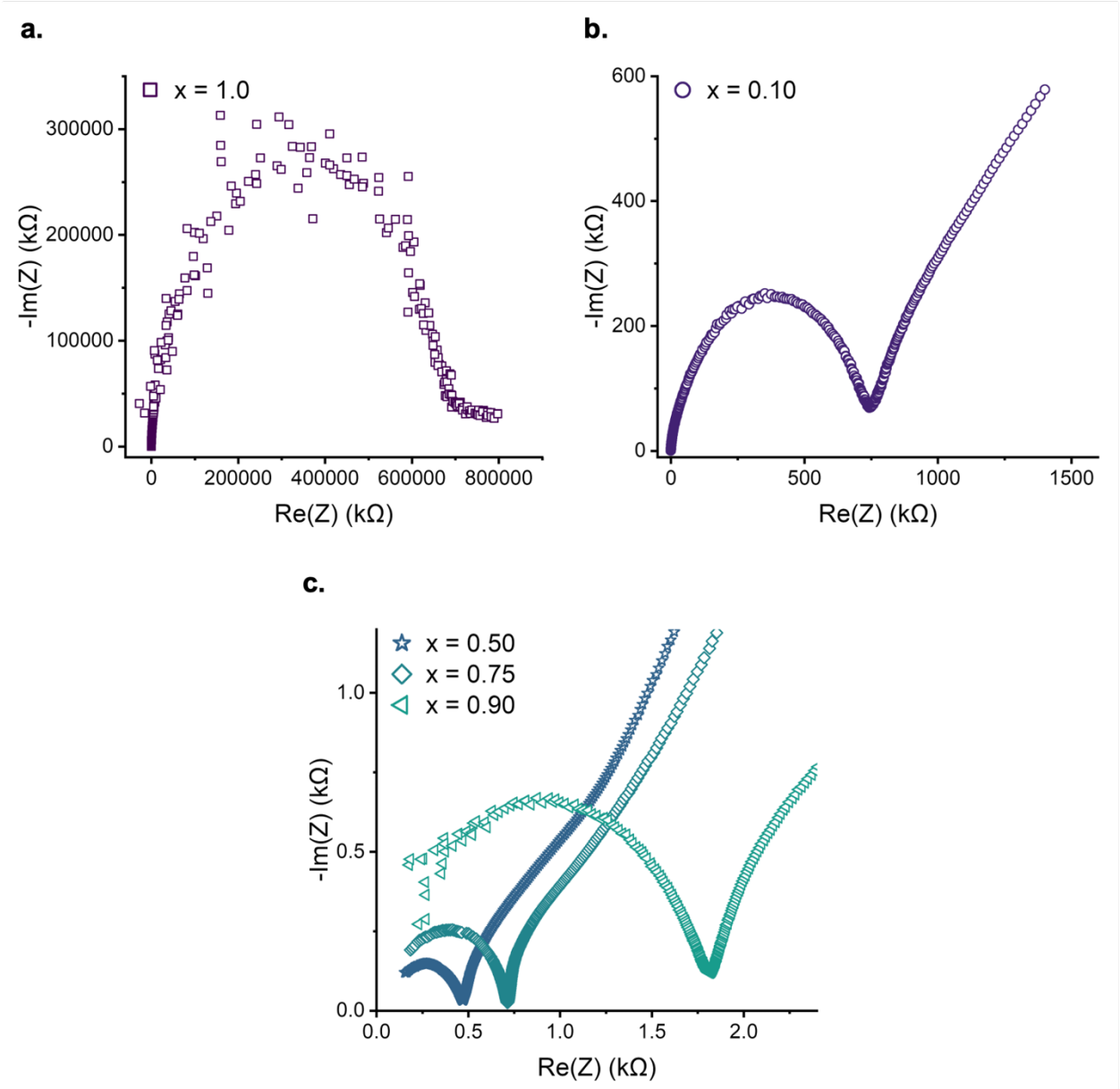

Figure S7. Nyquist plot of room temperature electrochemical impedance measurements for (a) YNb0, (b) YNb10, and (c) YNb50, YNb75, and YNb90.